Optics Communications 407 (2018) 57–62

Contents lists available at ScienceDirect

Optics Communications

journal homepage: www.elsevier.com/locate/optcom

Optical temperature sensing behavior of $Er^{3+}/Yb^{3+}/Tm^{3+}$:Y_2O_3 nanoparticles based on thermally and non-thermally coupled levels

Guangrun Chen, Ruoshan Lei *, Feifei Huang, Huanping Wang, Shilong Zhao, Shiqing Xu *

College of Materials Science and Engineering, China Jiliang University, Hangzhou 310018, China

ARTICLE INFO

Keywords:
Optical temperature sensing
Rare earth
Upconversion luminescence
FIR technique

ABSTRACT

$Er^{3+}/Yb^{3+}/Tm^{3+}$ triply doped Y_2O_3 nanoparticles have been synthesized by solute combustion method. X-ray diffraction (XRD) and scanning electron microscopy (SEM) demonstrate that the prepared particles are cubic Y_2O_3 phase with the average size of ~49 nm. The blue (Tm^{3+}:$^1G_4 \rightarrow {}^3H_6$), green ($Er^{3+}$:$^2H_{11/2}$,$^4S_{3/2} \rightarrow {}^4I_{15/2}$) and red ($Er^{3+}$:$^4F_{9/2} \rightarrow {}^4I_{15/2}$) upconversion (UC) emissions are observed upon a 980 nm excitation. Applying the fluorescence intensity ratio (FIR) technique, the optical temperature sensing behaviors are studied based on thermally coupled levels ($^2H_{11/2}$ and$^4S_{3/2}$ of Er^{3+}) and non-thermally coupled levels ($^1G_{4(b)}$ (Tm^{3+}) and$^2H_{11/2}$ (Er^{3+})), respectively. The results show that the absolute sensing sensitivity is much higher in the entire experimental temperature range, when the non-thermally coupled levels with different temperature dependences ($^1G_{4(b)}$ (Tm^{3+}) and$^2H_{11/2}$ (Er^{3+})) are selected as the thermometric index. The maximum absolute sensitivity is found to be as high as ~1640×10^{-4} K^{-1} at 573 K. This demonstrates that an optical temperature sensor with high performance can be designed based on the $Er^{3+}/Yb^{3+}/Tm^{3+}$:Y_2O_3 nanoparticles.

1. Introduction

In recent years, optical thermometer based on rare earth (RE) doped materials is a topic of extensive research owe to its particular applications in electromagnetical, thermal harsh and/or corrosive circumstances (i.e. coal mines, electrical power stations, oil refineries and so on) [1–4]. Among the optical temperature sensing methods, the FIR technique is considered as an extremely promising one. It commonly determines temperature via analysis of the emission intensity ratio between two thermally coupled energy levels, which can provide accurate measurements without influences of the fluorescence losses and pump power fluctuation [5–14]. By employing the FIR technique, the temperature sensing properties of many materials doped with RE^{3+} ions (i.e. Er^{3+}, Ho^{3+}, Tm^{3+} and Pr^{3+} etc.) have been reported by different researches [5–15]. For example, Bin Dong et al. have reported that Er–Mo:$Yb_3Al_5O_{12}$ nanoparticles exhibit the maximum sensing sensitivity of 48 × 10^{-4} K^{-1} at 467 K based on the thermally coupled levels $^2H_{11/2}$ and $^4S_{2/3}$ of Er^{3+}, which can be used as temperature sensor and in vivo imaging [16].

The temperature sensing sensitivity is an important parameter for an optical thermometer. Basically, a larger energy gap between the thermally coupled levels benefits the enhancement of sensitivity [9]. However, the largest energy mismatches between those two thermally coupled levels cannot exceed 2000 cm^{-1}, which blocks the further improvement of the sensing sensitivity [5,9]. Meanwhile, a large energy difference may lead to the "decoupling" effect at low temperature, which will introduce unavoidable measurement error [5]. Therefore, great efforts are still underway in the development of optical sensing materials with high sensitivity. Recently, several investigators have proposed that the optical sensor sensitivity can be enhanced effectively by using two non-thermal coupling levels from RE^{3+} ions [5,17–19]. For example, it is reported that the highest absolute sensitivity in $NaLuF_4$:$Yb^{3+}/Er^{3+}/Tm^{3+}$ nanoparticles is up to 604 × 10^{-4} K^{-1} at 300 K based on the non-thermal coupling levels ($^1D_2$ and $^1G_4$) of Tm^{3+} ions [5]. However, the reported absolute sensitivity value there is still smaller than that obtained in the present study.

Y_2O_3 has been widely applied as the host matrix of RE^{3+} ions for UC luminescence owe to its relatively low phonon energy (~430–550 cm^{-1}), excellent thermal conductivity and chemical durability etc. [20]. Recently, the color-tunable UC luminescence with high efficiency in $Er^{3+}/Yb^{3+}/Tm^{3+}$:Y_2O_3 using 980 nm excitation has been reported [21,22]. However, the temperature sensing behavior of $Er^{3+}/Yb^{3+}/Tm^{3+}$:Y_2O_3 nanoparticles are rarely investigated.

* Corresponding authors.
E-mail addresses: leiruoshan@cjlu.edu.cn (R. Lei), sxucjlu@163.com (S. Xu).

http://dx.doi.org/10.1016/j.optcom.2017.09.014
Received 15 June 2017; Received in revised form 23 August 2017; Accepted 5 September 2017
Available online 14 September 2017
0030-4018/

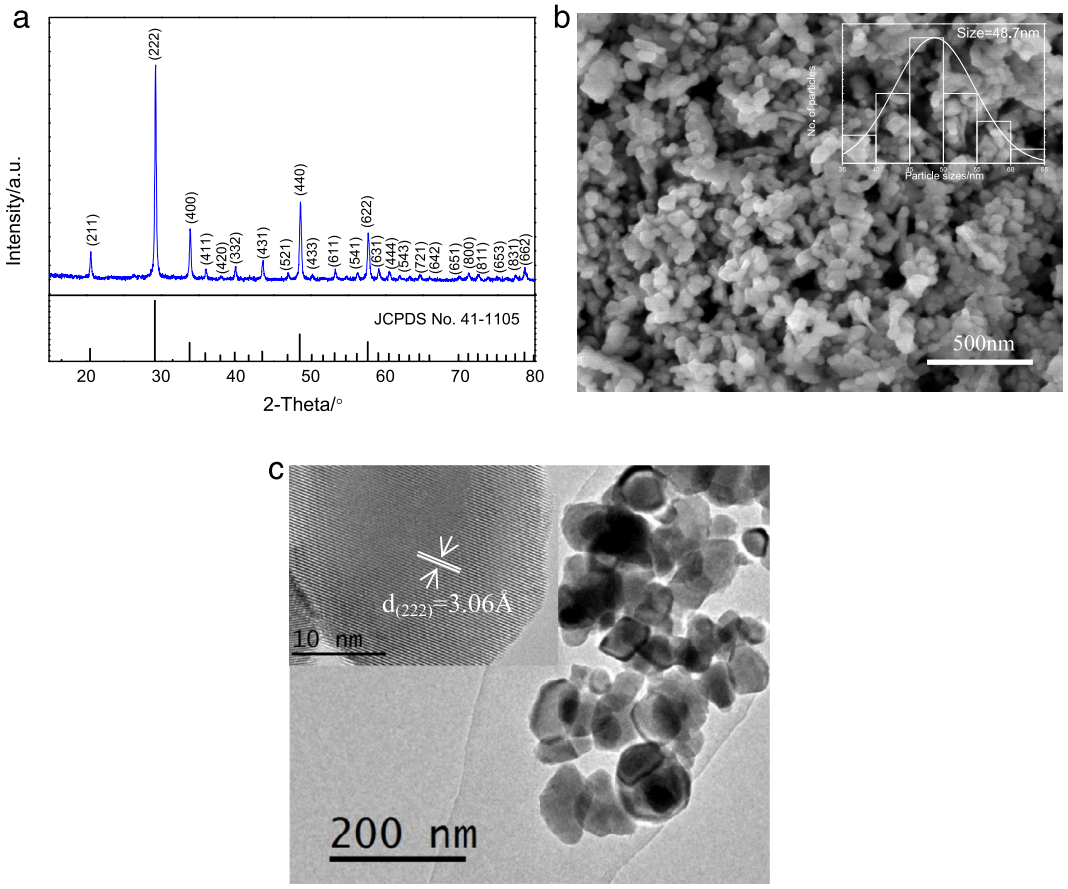

Fig. 1. (a) XRD pattern of the synthesized Y_2O_3:0.5%Er^{3+}/3%Yb^{3+}/0.1%Tm^{3+} nanoparticles (top) with JCPDS No. 41-1105 (bottom). SEM image (b) and TEM image (c) of Y_2O_3:0.5%Er^{3+}/3%Yb^{3+}/0.1%Tm^{3+} nanoparticles, respectively. The histogram of the particle size distribution and HRTEM image of the sample have been shown in the inset of Fig. 1(b) and (c), respectively.

In this work, Y_2O_3: 0.5%Er^{3+}/3%Yb^{3+}/0.1%Tm^{3+} nanoparticles have been synthesized by using solute combustion method. The structure and morphology of the nanoparticles have been studied by XRD, SEM and transmission electron microscopy (TEM) observations. The UC luminescent property is investigated upon 980 nm excitation. More importantly, the optical temperature sensing behaviors utilizing the FIR technique have been studied based on thermally coupled levels ($^2H_{11/2}$ and $^4S_{3/2}$ of Er^{3+}) and non-thermally coupled levels ($^1G_{4(b)}$ of Tm^{3+} and $^2H_{11/2}$ of Er^{3+}), respectively.

2. Experimental

Y_2O_3: 0.5%Er^{3+}/3%Yb^{3+}/0.1%Tm^{3+} nanoparticles were synthesized by solute combustion method. $Y(NO_3)_3\cdot 6H_2O$, $Er(NO_3)_3\cdot 5H_2O$, $Tm(NO_3)_3\cdot 6H_2O$ and $Yb(NO_3)_3 6H_2O$ with high purity (99.9%–99.99%) were dissolved in the deionized water, respectively. These solutions were mixed and stirred in accordance with the appropriate ratio. Glycine as complexing agent was added by keeping the nitrate to glycine ratio 1:3.5. Then, the solution pH was adjusted to 6 by adding ammonium water. The final solution was heated in air at 90 °C to convert into a glassy gel, which was further heated at a temperature of 450 °C to form white foamy powders. In order to increase the crystallinity and eliminate the impurities, the powders were finally calcined at 1000 °C for 2 h.

XRD analysis was performed using a X-ray diffractometer (Bruker D2 PHASER Diffractometer) with Cu–K_α radiation (λ = 1.5406 Å). SEM images were taken on a HITACHI TM 3000 operating at 50 kV. A Tecnai G2 F20 transmission electron microscope was used to perform the TEM and high resolution TEM (HRTEM) observations, which operates at a voltage of 200 kV. The measurements of UC photoluminescence (PL) spectra were carried out on a FLUOROLOG3/ Jobin-Yvon spectrofluorometer under a 980 nm diode laser excitation. A temperature controlling system (TAP-02) was used to adjust the sample temperatures from room temperature to 573 K.

3. Results and discussion

Fig. 1(a) shows the XRD pattern of the synthesized Y_2O_3:0.5%Er^{3+}/3%Yb^{3+}/0.1%Tm^{3+} nanoparticles. It can be seen that all the diffraction peaks of the sample match well with the standard pattern of cubic Y_2O_3 phase (JCPDS No. 41-1105), and no extra impurity phases can be observed, suggesting the formation of phase pure material. The average grain size is calculated to be ~45 nm via the Scherrer's equation [23].

In order to investigate the morphological feature and particle size of the Y_2O_3:0.5%Er^{3+}/3%Yb^{3+}/0.1%Tm^{3+} nanoparticles, SEM and TEM observations were carried out. As shown in Fig. 1(b), the nanoparticles exhibit relatively irregular morphology with the mean particle size to be ~49 nm, which is in agreement with the XRD result. The TEM image (Fig. 1(c)) further confirms that the obtained phosphors are made of the crystalline grains with sizes of 35–65 nm. Moreover, the HRTEM image (inset of Fig. 1(c)) clearly verifies that the particle is highly crystallized with long-range order. The obvious lattice fringes with the d -spacing around 3.06 Åis corresponding to the (222) plane of cubic Y_2O_3.

Fig. 2(a) shows the room temperature UC emission spectrum of Y_2O_3:0.5%Er^{3+}/3%Yb^{3+}/0.1%Tm^{3+} nanoparticles under a 980 nm excitation with pump power of 150 mW. Three distinct emission bands in blue, green and red regions are detected. The characteristic emissions peaked at 477 and 490 nm can be ascribed to $^1G_4 \rightarrow^3 H_6$ transition of Tm^{3+} ion, while the peaks centered at 541, 566 and 662 nm

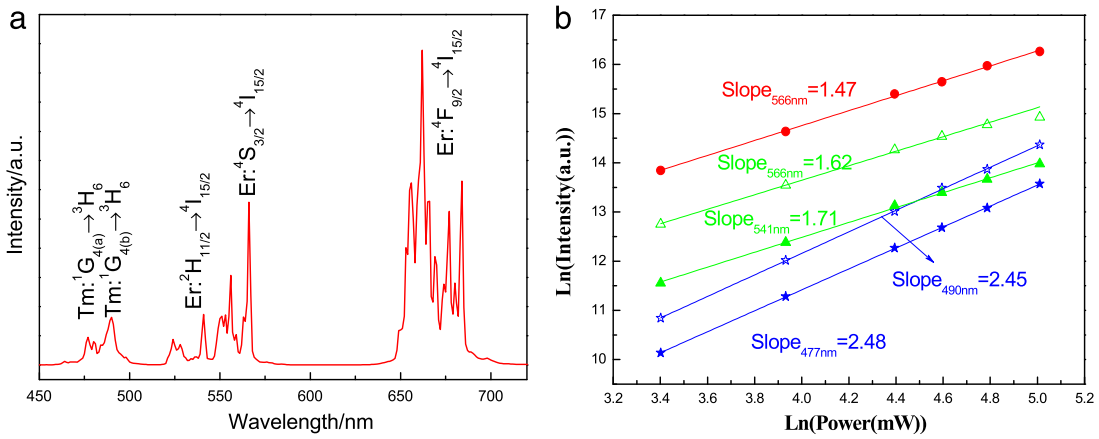

Fig. 2. (a) UC emission spectrum of 0.5%Er^{3+}/3%Yb^{3+}/0.1%Tm^{3+}: Y_2O_3 nanoparticles; (b) The log–log plots of UC emission intensity as a function of the pump power of a 980 nm laser.

are corresponding to the $^2H_{11/2} \rightarrow {}^4I_{15/2}$, $^4S_{3/2} \rightarrow {}^4I_{15/2}$ and $^4F_{9/2} \rightarrow {}^4I_{15/2}$ transitions of Er^{3+} ions, respectively. Fig. 2(b) shows log–log plots of UC emission intensity as a function of the pump power for different emissions. The slope value of the curves represents the number of the pump photons involved to populate the upper emitting state for the unsaturated condition [24]. The results demonstrate that the green and red transitions are two-photon process, while the blue transition comes from three-photon UC process. Furthermore, the slope values for the blue emissions at 477 and 490 nm are 2.48 and 2.45 respectively, suggesting that the two bands are originated from the Stark sublevels of $^1G_{4(a)} \rightarrow {}^3H_6$ and $^1G_{4(b)} \rightarrow {}^3H_6$, respectively. The splitting of $^1G_4$ level due to the crystal field effect has been discussed previously [17].

The possible UC processes have been depicted in the simplified energy level diagram shown in Fig. 3. Under 980 nm optical excitation, Yb^{3+} ions can be excited to $^2F_{5/2}$ state by ground state absorption (GSA) process, and then the sequential energy transfer (ET) processes from Yb^{3+} to Er^{3+} and Tm^{3+} ions play vital roles in the populations of the excited states of Er^{3+} and Tm^{3+}. For Tm^{3+} ions, the sequential ET1, ET2 and ET3 processes from Yb^{3+} to Tm^{3+} ions mainly contribute to the population of $^1G_4$ state. Finally, the $^1G_4 \rightarrow {}^3H_6$ transition gives rise to the blue emission. Hence, the blue UC emission of Tm^{3+} ions comes from three-photon process. However, the slope value for the blue UC emission shown in Fig. 2(b) is smaller than the excepted value (~3). This might be resulted from cooperative energy transfer (CET) from Yb^{3+} to Tm^{3+} ions [18]. As shown in Fig. 3, a pair of neighboring Yb^{3+} ions in the excited $^2F_{5/2}$ level can transfer their energy simultaneously to a Tm^{3+} ion, resulting in the excitation of Tm^{3+} ion to the $^1G_4$ state (CET1). As the CET process is a two-photon process, the slope value of blue emission becomes lower than the expected value. For Er^{3+} ions, they are excited to the $^4F_{7/2}$ state via the sequential ET4 and ET5. Besides, the $^4F_{7/2}$ state may also be populated via CET2 [25]. And then the Er^{3+} ions can nonradiatively transmit to the states of $^2H_{11/2}$ and $^4S_{3/2}$. Accordingly, the green emissions are generated by the transitions of $^2H_{11/2} \rightarrow {}^4I_{15/2}$ and $^4S_{3/2} \rightarrow {}^4I_{15/2}$ of Er^{3+} ions. Alternatively, the Er^{3+} ions at the $^4S_{3/2}$ state can nonradiatively relax to the $^4F_{9/2}$ state. Also, the $^4F_{9/2}$ state can be populated by the combination of the non-radiative relaxation process ($^4I_{11/2} \rightarrow {}^4I_{13/2}$) and the ET6 process ($^4I_{13/2} + {}^2F_{5/2} \rightarrow {}^4F_{9/2}$). Finally, the transition of $^4F_{9/2} \rightarrow {}^4I_{15/2}$ results in the red emission.

The optical temperature sensor property of Y_2O_3: 0.5%Er^{3+}/3%Yb^{3+}/0.1%Tm^{3+} nanoparticles is investigated in the temperature range of 298–573 K with a 980 nm pump power of 99 mW. The temperature-dependent UC green luminescent spectra are normalized to 566 nm peak, as shown in Fig. 4(a). The emission intensity from $^2H_{11/2} \rightarrow {}^4I_{15/2}$ transition enhances gradually with respect to that from $^4S_{3/2} \rightarrow {}^4I_{15/2}$ transition with increasing temperatures. This is because $^2H_{11/2}$ and $^4S_{3/2}$ of Er^{3+} ions are thermally coupled levels with small

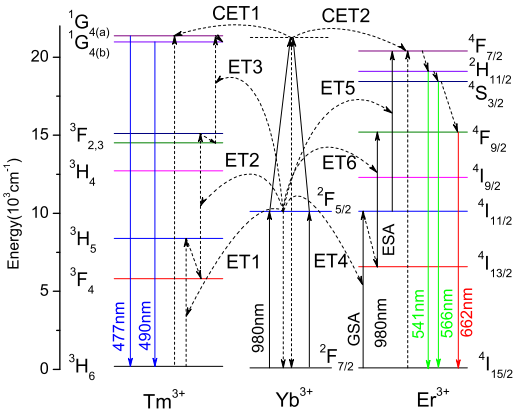

Fig. 3. Energy level diagram as well as the possible UC mechanisms under 980 nm excitation.

energy gap of ~700 cm^{-1}, resulting in the population redistribution from the lower energy level ($^4S_{3/2}$) to the higher one ($^2H_{11/2}$) [2].

Similarly, Fig. 4(b) reveals that the emission band ranging from 520–545 nm ($^2H_{11/2} \rightarrow {}^4I_{15/2}$ of Er^{3+}) increases considerably with the increment of temperature, when the emission intensity is normalized at 490 nm ($^1G_{4(b)} \rightarrow {}^3H_6$ of Tm^{3+}). To better illustrate the temperature dependence, Fig. 4(c) shows the intensity variations of the bands peaked at 490 and 541 nm as a function of temperature. It can be noticed that the intensity of $^1G_{4(b)} \rightarrow {}^3H_6$ transition of Tm^{3+} ions decreases sharply with the increasing temperature. Several reasons can be taken into consideration. Firstly, the non-radiative relaxation rate becomes fast with increasing temperatures, leading to the depopulation of $^1G_{4(b)}$ level. A second explanation for the intensity reduction of $^1G_{4(b)} \rightarrow {}^3H_6$ transition is related to the thermal excitation process of $^1G_{4(b)} \rightarrow {}^1G_{4(a)}$, since the two levels are closely spaced [17]. In addition, the phonon-assisted ET processes between Er^{3+} and Tm^{3+} ions, such as $^1G_4$ (Tm^{3+}) + $^4I_{11/2}$ (Er^{3+}) → $^3H_4$ (Tm^{3+}) + $^2H_{11/2}$ (Er^{3+}) and $^1G_4$ (Tm^{3+}) + $^4I_{9/2}$ (Er^{3+}) → $^3F_{2,3}$ (Tm^{3+}) + $^2H_{11/2}$ (Er^{3+}), are reported to become efficient with increment of temperature [26], which also depopulate $^1G_4$ level. On the contrary, the intensity of $^2H_{11/2} \rightarrow {}^4I_{15/2}$ transition increases when the temperatures rise from 298 to 423 K. As stated above, the thermal population of $^2H_{11/2}$ level from the lower $^4S_{3/2}$ level takes place with increasing temperature, which is predominant to promote the radiative transition of $^2H_{11/2} \rightarrow {}^4I_{15/2}$. Additionally, the above said ET processes between Er^{3+} and Tm^{3+} ions may be the minor mechanism for populating the $^2H_{11/2}$ level. However, when the temperature increases further, the population of $^2H_{11/2}$ is blocked via the enhanced non-radiative

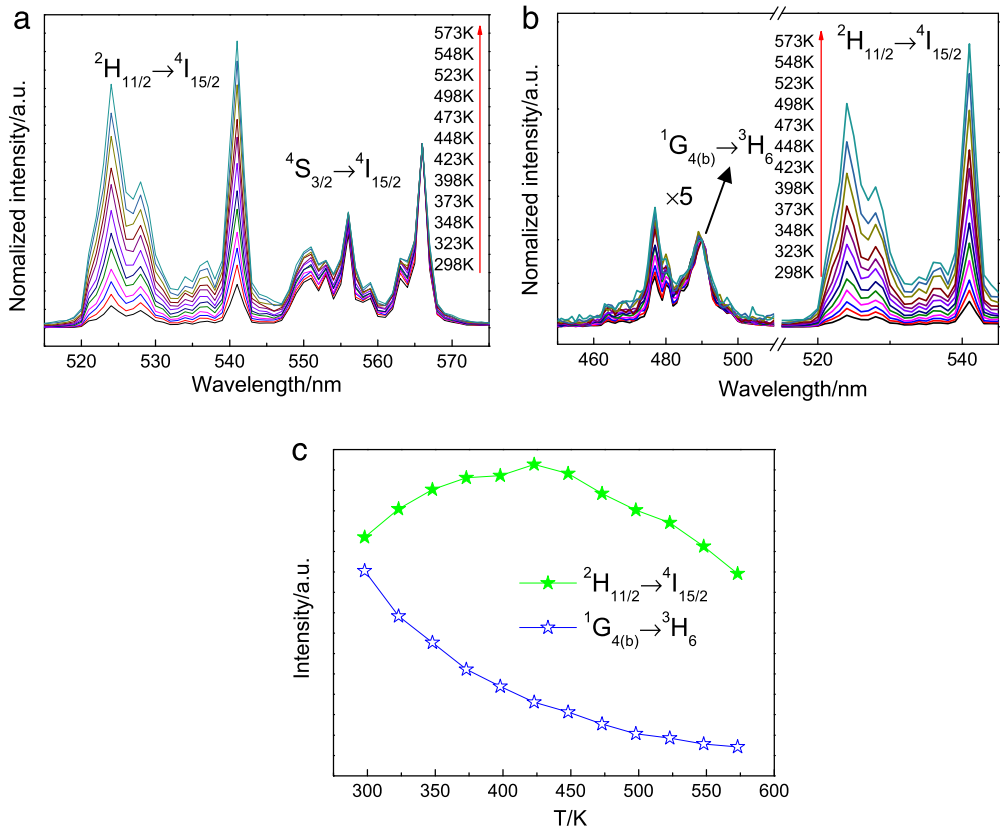

Fig. 4. (a) Normalized green UC spectra at different temperatures, where the emission intensity was normalized at 566 nm. (b) Variation of the bands peaked at 490 and 541 nm with temperature. The intensities are normalized to the peak around 490 nm. (c) The temperature dependent integral intensities of the bands peaked at 490 and 541 nm. (For interpretation of the references to color in this figure legend, the reader is referred to the web version of this article.)

relaxation process, leading to the reduction of emission intensity at higher temperatures. Overall, the $^1G_{4(b)}\rightarrow{}^3H_6$ (Tm^{3+}) and $^2H_{11/2}\rightarrow{}^4I_{15/2}$ (Er^{3+}) emissions exhibit the diverse temperature dependences, hence, the intensity ratio of the two emissions can be applied as an index for probing temperature.

Based on the Boltzmann distribution theory, the FIR for the thermally coupled levels can be calculated as follows [8,27]:

$$FIR = \frac{I_a}{I_b} = C\exp\left(\frac{-\Delta E}{kT}\right) \tag{1}$$

where I is integrated intensities of emission bands. ΔE is the energy gap between two thermally coupled levels, C and k are a pre-exponential constant and Boltzmann constant (0.695 K^{-1}), respectively. T is the absolute temperature.

Accordingly, the intensity ratio arising from the thermally coupled levels of $^2H_{11/2}$ (541 nm) and $^4S_{3/2}$ (566 nm) of Er^{3+} ions can be well fitted to the following equation (Fig. 5(a)):

$$FIR = I_{541}/I_{566} = 11.7exp(-1124/T). \tag{2}$$

This demonstrates that the parameters C and $\Delta E/k$ are ~11.7 and 1124 K, respectively. Accordingly, the energy gap between $^2H_{11/2}$ and $^4S_{3/2}$ levels can be calculated to be ~781 cm^{-1}, which matches well with the actual value of ~700 cm^{-1}.

On the other hand, as the $^1G_{4(b)}$ (Tm^{3+}) and $^2H_{11/2}$ (Er^{3+}) levels are non-thermally coupled levels, Eq. (1) is not suitable to express the temperature dependence of FIR values originated from $^2H_{11/2}\rightarrow{}^4I_{15/2}$ (541 nm) and $^1G_{4(b)}\rightarrow{}^3H_6$ (490 nm) transitions [17]. Otherwise, Chen et al. [28] and Zhou et al. [17] have proposed that the FIR data from two non-thermally coupled levels can be fitted by the following exponential equation:

$$FIR = A\exp(-B/T) + C \tag{3}$$

where T presents the absolute temperature. A, B and C are constants, which are evaluated by fitting the experimental data. Based on Eq. (3), the best fit of FIR value (I_{541}/I_{490}) to temperature is as follows:

$$FIR = I_{541}/I_{490} = 2215.8exp(-2697.7/T) + 1.3. \tag{4}$$

As shown in Fig. 5(a), the correlation coefficient R is as high as ~0.995, revealing a perfect fitting is achieved. Hence, the temperature can be accurately detected with the help of the intensity ratio between $^2H_{11/2}\rightarrow{}^4I_{15/2}$ (Er^{3+}) and $^1G_{4(b)}\rightarrow{}^3H_6$ (Tm^{3+}) transitions.

What is more, it is important to know the sensor sensitivity of the sample for optical thermometry applications. The absolute sensor sensitivity (S_a) presents the change rate of FIR with response to the temperature variation, which is defined as [2,16]:

$$S_a = \frac{dFIR}{dT}. \tag{5}$$

While the relative sensor sensitivity (S_r) is the normalized S_a with respect to the measured FIR value, which is expressed as [29]:

$$S_r = \frac{1}{FIR}\frac{dFIR}{dT}. \tag{6}$$

Fig. 5(b) shows the corresponding S_a curves as a function of temperature. It is revealed that the S_a value of the optical thermometer based on non-thermally coupled levels ($^1G_{4(b)}$ (Tm^{3+}) and $^2H_{11/2}$ (Er^{3+})) is much higher than that based on thermally coupled levels ($^2H_{11/2}$ and $^4S_{3/2}$ of Er^{3+}) in the whole experimental temperature range. On the other hand, the dependences of the calculated S_r values on temperature are given in Fig. 5(c). As shown, although the S_r value based on $^1G_{4(b)}$ (Tm^{3+}) and $^2H_{11/2}$ (Er^{3+}) levels is lower than that based on $^2H_{11/2}$ and $^4S_{3/2}$ levels of Er^{3+} at the temperatures lower than 348 K, a reverse trend occurs at higher temperatures. Noteworthily, in the case of non-thermal coupling levels ($^1G_{4(b)}$ (Tm^{3+}) and $^2H_{11/2}$ (Er^{3+})), the maximal value of S_a is

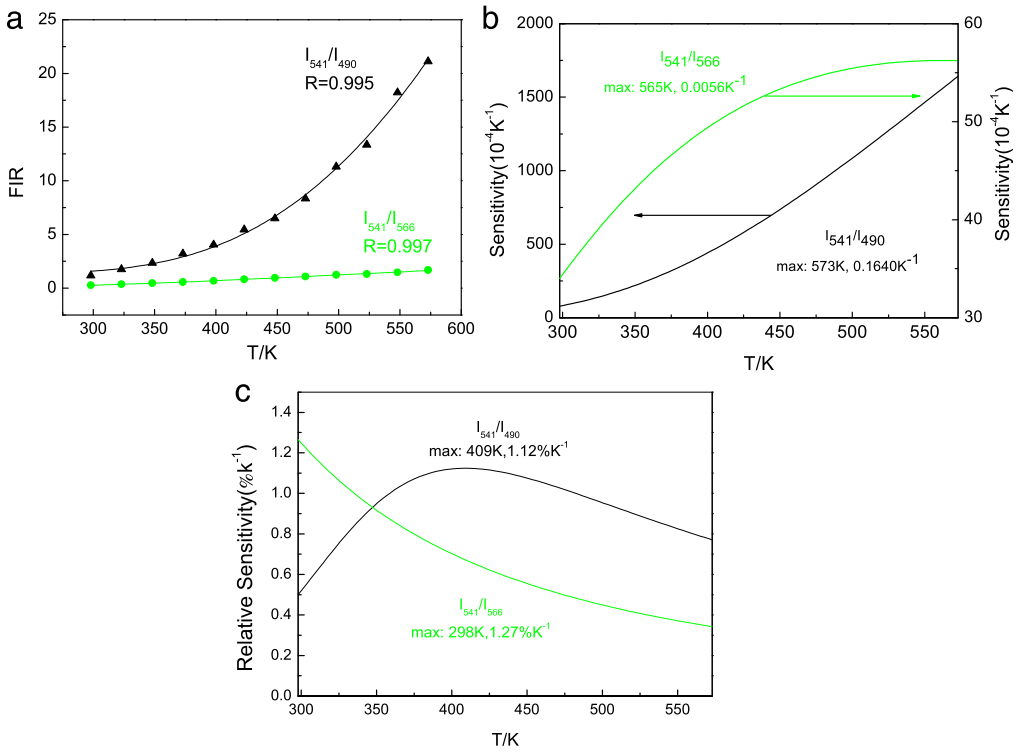

Fig. 5. (a) Plots of FIR based on thermally coupled levels ($^2H_{11/2}$ and $^4S_{2/3}$) and non-thermally coupled levels ($^1G_{4(b)}$) and $^2H_{11/2}$ as a function of temperature. *R* represents the correlation coefficient. The evolutions of S_a (b) and S_r values (c) based on thermally coupled levels and non-thermally coupled levels as a function of temperature, respectively.

Table 1
Optical sensing sensitivities of different materials doped with RE^{3+} ions.

Sample	Transitions	S_a (10^{-4} K^{-1})	S_r (%K^{-1})	T (K)	Reference
Tm/Yb/Er:Y_2O_3	$^2H_{11/2}$, $^4S_{3/2}$ →^{4} $I_{15/2}$	56	1.27	298–573	This work
	$^2H_{11/2}$ →^{4} $I_{15/2}$, $^1G_{4(b)}$ →^{3} H_6	1640	1.12	298–573	This work
Er/Yb:$NaLuF_4$	$^2H_{11/2}$, $^4S_{3/2}$ →^{4} $I_{15/2}$	52	/	303–523	[30]
Er/Yb:ZnO–$CaTiO_3$	$^2H_{11/2}$, $^4S_{3/2}$→$^4I_{15/2}$	105	1.16	300–700	[31]
Er/Yb:$NaYF_4$	$^2H_{11/2}$, $^4S_{3/2}$ →^{4} $I_{15/2}$	/	1.20	160–300	[32]
Ho/Yb:$CaWO_4$	$^5F_{2,3}$/$^3K_8$, $^5G_6$/$^5G_1$→$^5I_8$	205	0.5	300–690	[33]
Yb/Er/Tm:YF_3	$^2H_{11/2}$, $^4S_{3/2}$ →^{4} $I_{15/2}$	/	1.01	293–563	[34]
α-$NaYF_4$: Tm/Yb @CaF_2	$^3H_{4(a)}$, $^3H_{4(b)}$→$^3H_6$	43	/	313–373	[35]

as high as ~1640 × 10^{-4} K^{-1} at 573 K, while that of S_r is ~1.12%K^{-1} at 409 K. This performance is superior to those typical RE^{3+} doped materials based on thermally coupled levels, as illustrated in Table 1. Hence, the strategy of using the intensity ratio between $^2H_{11/2}$→$^4I_{15/2}$ (Er^{3+}) and $^1G_{4(b)}$→$^3H^6$ (Tm^{3+}) in Y_2O_3 nanoparticles is a promising way for high performed temperature sensing.

4. Conclusion

In summary, 0.5%Er^{3+}/3%Yb^{3+}/0.1%Tm^{3+}:Y_2O_3 nanoparticles were prepared by solution combustion method. The XRD, SEM and TEM results reveal that the product is cubic phase of Y_2O_3 with high crystallinity and the mean particle size is ~49 nm. The UC emissions in the spectral range from blue to red were obtained under a 980 nm excitation. Using the FIR technique, the optical temperature sensing behaviors of the nanoparticles were discussed based on thermally coupled levels ($^2H_{11/2}$ and $^4S_{3/2}$ of Er^{3+}) and non-thermally coupled levels ($^1G_{4(b)}$ (Tm^{3+}) and $^2H_{11/2}$ (Er^{3+})), respectively. The results illustrate that the absolute sensitivity based on $^2H_{11/2}$→$^4I_{15/2}$ and $^1G_{4(b)}$→$^3H_6$ transitions with different temperature dependences is higher in the temperature range from 298 to 573 K. The maximum absolute sensitivity can reach as high as 1640 × 10^{-4} K^{-1} at 573 K. Hence, the 0.5%Er^{3+}/3%Yb^{3+}/0.1%Tm^{3+}:Y_2O_3 nanoparticles show a potential application value in optical thermometry due to the high sensing sensitivity.

Acknowledgments

Project supported by the National Science Foundation of China (No. 51401197 and 61605192) and the Natural Science Foundation of Zhejiang Province (LR15F050003 and LZ14B010001).

References

[1] S.P. Haro-González, K. Horchani-Naifer, M. Férida, La_2O_3: Tm, Yb, Er upconverting nano-oxides for sub-tissue life time thermally sensing, Sensors Actuators B 234 (2016) 541–548.
[2] Z. Sun, G.F. Liu, Z.L. Fu, T.Q. Sheng, Y.L. Wei, Z.J. Wu, Nanostructured La_2O_3: Yb^{3+}/Er^{3+}: temperature sensing, optical heating and bio-imaging application, Mate. Res. Bull. 92 (2017) 39–45.
[3] J. Wang, L.H. Luo, Y.P. Huang, W.P. Li, Effect of Yb codoping on the phase transition, and electrical and photoluminescence properties in KNLN: Er/xYb ceramics, J. Am. Ceram. Soc. 99 (2016) 1625–1630.
[4] Y.P. Huang, L.H. Luo, Up-conversion photoluminescence based on the intrinsic defects in $Na_{0.5}Bi_{0.5}TiO_3$: Yb^{3+} ceramics, J. Alloys Compd. 706 (2017) 312–317.
[5] H.Y. Lu, H.Y. Hao, G. Shi, Y.C. Gao, R.X. Wang, Y.L. Song, Y.X. Wang, X.R. Zhang, Optical temperature sensing in β-$NaLuF_4$:Yb^{3+}/Er^{3+}/Tm^{3+} based on thermal, quasi-thermal and non-thermal coupling levels, RSC Adv. 6 (2016) 55307–55311.
[6] A. Sedlmeier, D.E. Achatz, L.H. Fischer, H.H. Gorris, O.S. Wolfbeis, Photon upconverting nanoparticles for luminescent sensing of temperature, Nanoscale. 4 (2012) 7090–7096.
[7] Z. Wei, W. Zheng, Z.Y. Zhu, X.F. Guo, Upconversion of $SrWO_4$:Er^{3+}/Yb^{3+}: Improvement by Yb^{3+} codoping and temperature sensitivity for optical temperature sensors, Chem. Phys. Lett. 651 (2016) 46–49.

[8] F. Huang, Y. Gao, J.C. Zhou, J. Xu, Y.S. Wang, Yb^{3+}/Er^{3+} co-doped $CaMoO_4$: a promising green upconversion phosphor for optical temperature sensing, J. Alloys Compd. 639 (2015) 325–329.
[9] A.F. Pereira, K.U. Kumar, W.F. Silva, W.Q. Santos, D. Jaque, C. Jacinto, Yb^{3+}/Tm^{3+} co-doped $NaNbO_3$ nanocrystals as three-photon-excited luminescent nanothermometers, Sensors Actuators B 213 (2015) 65–71.
[10] Q.H. Zuo, L.H. Luo, Y.J. Yao, High dielectric, piezoelectric, upconversion photoluminescence and low-temperature sensing properties in $Ba_{0.7}Sr_{0.3}TiO_3$-$BaZr_{0.2}Ti_{0.8}O_3$: Ho/Yb ceramics, J. Electron. Mater. 45 (2016) 970–975.
[11] V.K. Rai, D.K. Rai, S.B. Rai, Pr^{3+} doped lithium tellurite glass as a temperature sensor, Sens. Actuators A: Phys. 128 (2006) 14–17.
[12] D.Q. Chen, M. Xu, S. Liu, X.Y. Li, Eu^{2+}/Eu^{3+} dual-emitting glass ceramic for self-calibrated optical thermometry, Sensors Actuators B 246 (2017) 756–760.
[13] D.Q. Chen, S. Liu, Z.Y. Wang, Z.G. Ji, EuF_3/Ga_2O_3 dual-phase nanostructural glass ceramics with Eu^{2+}/Cr^{3+} dual-activator luminescence for self-calibrated optical thermometry, J. Phys. Chem. C 120 (2016) 21858–21865.
[14] M. Xu, D.Q. Chen, P. Huang, Z.Y. Wan, Y. Zhou, Z.G. Ji, A dual-functional upconversion core@ shell nanostructure for white-light-emission and temperature sensing, J. Mater. Chem. C 4 (2016) 6516–6524.
[15] R.K. Verma, S.B. Rai, Laser induced optical heating from Yb^{3+}/Ho^{3+}:$Ca_{12}Al_{14}O_{33}$ and its applicability as a thermal probe, J. Quant. Spectrosc. RA. 113 (2012) 1594–1600.
[16] B. Dong, B.S. Cao, Y.Y. He, Z. Liu, Z.P. Li, Z.Q. Feng, Temperature sensing and in vivo imaging by molybdenum sensitized visible upconversion luminescence of rare-earth oxides, Adv. Mater. 24 (2012) 1987–1993.
[17] S.S. Zhou, G.C. Jiang, X.Y. Li, S. Jiang, X.T. Wei, Y.H. Chen, M. Yin, C.K. Duan, Strategy for thermometry via Tm^{3+}-doped $NaYF_4$ core–shell nanoparticles, Opt. Lett. 39 (2014) 6687–6690.
[18] A. Pandey, V.K. Rai, Optical thermometry using FIR of two close lying levels of different ions in Y_2O_3:Ho^{3+}-Tm^{3+}-Yb^{3+} phosphor, Appl. Phys. B 113 (2013) 221–225.
[19] D.Q. Chen, S. Liu, Y. Zhou, Z.Y. Wan, P. Huang, Z.G. Ji, Dual-activator luminescence of RE/TM: $Y_3Al_5O_{12}$ (RE = Eu^{3+}, Tb^{3+}, Dy^{3+}; TM = Mn^{4+}, Cr^{3+}) phosphors for self-referencing optical thermometry, J. Mater. Chem. C 4 (2016) 9044–9051.
[20] T. Fan, J.T. Lü, Enhanced 1.5 μm and green upconversion emissions in Y_2O_3:Er^{3+} nanoparticles codoped with Li^+ ions, Opt. Commun. 300 (2013) 5–7.
[21] Y.F. Bai, Y.X. Wang, G.Y. Peng, W. Zhang, Y.K. Wang, K. Yang, X.R. Zhang, Y.L. Song, Enhanced white light emission in Er/Tm/Yb/Li codoped Y_2O_3 nanocrystals, Opt. Commun. 282 (2009) 1922–1924.
[22] X.R. Hou, S.M. Zhou, T.T. Jia, H. Lin, H. Teng, White light emission in $Tm^{3+}/Er^{3+}/Yb^{3+}$ tri-doped Y_2O_3 transparent ceramic, J. Alloys Compd. 509 (2011) 2793–2796.
[23] P. Packiyaraj, P. Thangadurai, Structural and photoluminescence studies of Eu^{3+} doped cubic Y_2O_3 nanophosphors, J. Lumin. 145 (2014) 997–1003.
[24] R. Dey, V.K. Rai, Yb^{3+} sensitized Er^{3+} doped La_2O_3 phosphor in temperature sensors and display devices, Dalton T. 43 (2014) 111–118.
[25] A. Pandey, V.K. Rai, V. Kumar, V. Kumar, H.C. Swart, Upconversion based temperature sensing ability of Er^{3+}-Yb^{3+} codoped $SrWO_4$: An optical heating phosphor, Sensors Actuators B 209 (2015) 352–358.
[26] N. Rakov, G.S. Maciel, Cooling of Er^{3+} with Tm^{3+} for accurate temperature sensing using yttrium silicate compact powders, Dalton Trans. 43 (2014) 16025–16030.
[27] D.Q. Chen, Z.Y. Wan, Y. Zhou, X.Z. Zhou, Y.L. Yu, J.S. Zhong, M.Y. Ding, Z.G. Ji, Dual-phase glass ceramic: structure, dual-modal luminescence, and temperature sensing behaviors, ASC Appl. Mater. Interfaces 7 (2015) 19484–19493.
[28] D.Q. Chen, S. Liu, Z.Y. Wan, Y. Chen, A highly sensitive upconverting nano-glass-ceramic-based optical thermometer, J. Alloys Compd. 672 (2016) 380–385.
[29] D.Q. Chen, M. Xu, P. Huang, Core@ shell upconverting nanoarchitectures for luminescent sensing of temperature, Sensors Actuators B 231 (2016) 576–583.
[30] K.Z. Zheng, W.Y. Song, G.H. He, Z. Yuan, W.P. Qin, Five-photon UV upconversion emission of Er^{3+} for temperature sensing, Opt. Express 23 (2015) 7653–7658.
[31] S.P. Tiwari, M.K. Mahata, K. Kumar, V.K. Rai, Enhanced temperature sensing response of upconversion luminescence in ZnO-$CaTiO_3$: Er^{3+}/Yb^{3+} nano-composite phosphor, Spectrochim. Acta. A. Mol. Biomol. Spectrosc. 150 (2015) 623–630.
[32] S.S. Zhou, K.M. Deng, X.T. Wei, G.C. Jiang, C.K. Duan, Y.H. Chen, M. Yin, Upconversion luminescence of $NaYF_4$: Yb^{3+}, Er^{3+} for temperature sensing, Opt. Commun. 291 (2013) 138–142.
[33] W. Xu, H. Zhao, Y.X. Li, L.J. Zheng, Z.G. Zhang, W.W. Cao, Optical temperature sensing through the upconversion luminescence from Ho^{3+}/Yb^{3+} codoped $CaWO_4$, Sensors Actuators B 188 (2013) 1096–1100.
[34] D.Q. Chen, S. Liu, X.Y. Li, S. Yuan, P. Huang, Upconversion luminescence based dual-modal temperature sensing for $Yb^{3+}/Er^{3+}/Tm^{3+}$: YF_3 nanocrystals embedded glass ceramic, J. Euro. Ceram. Soc. 37 (2007) 4939–4945.
[35] R.Z. Wu, J.J. Zhou, L. Lei, S.J. Zhang, Z. Xiao, J.J. Zhang, S.Q. Xu, α-$NaYF_4$: Yb^{3+}-Tm^{3+} @ CaF_2 nanocrystals for NIR to NIR temperature sensing, Chem. Phys. Lett. 667 (2017) 206–210.